Magnetized relativistic jets and long-duration GRBs from magnetar spin-down during core-collapse supernovae

N. Bucciantini,[1]⋆ E. Quataert,[1,2] B. D. Metzger,[1,2] T. A. Thompson,[3] J. Arons[1,2] and L. Del Zanna[4]

[1]*Astronomy Department and Theoretical Astrophysics Center, University of California, Berkeley, 601 Campbell Hall, Berkeley, CA 94720, USA*
[2]*Department of Physics, University of California, Berkeley, Le Conte Hall, Berkeley, CA 94720, USA*
[3]*Department of Astronomy and Center for Cosmology & Astro-Particle Physics, The Ohio State University, Columbus, OH 43210, USA*
[4]*Dipartimento di Astronomia e Scienza dello Spazio, Università di Firenze, L.go Fermi 2, 50125 Firenze, Italy*

ABSTRACT

We use ideal axisymmetric relativistic magnetohydrodynamic simulations to calculate the spin-down of a newly formed millisecond, $B \sim 10^{15}$ G, magnetar and its interaction with the surrounding stellar envelope during a core-collapse supernova (SN) explosion. The mass, angular momentum and rotational energy lost by the neutron star are determined self-consistently given the thermal properties of the cooling neutron star's atmosphere and the wind's interaction with the surrounding star. The magnetar drives a relativistic magnetized wind into a cavity created by the outgoing SN shock. For high spin-down powers ($\sim 10^{51}$–10^{52} erg s^{-1}), the magnetar wind is superfast at almost all latitudes, while for lower spin-down powers ($\sim 10^{50}$ erg s^{-1}), the wind is subfast but still super-Alfvénic. In all cases, the rates at which the neutron star loses mass, angular momentum and energy are very similar to the corresponding free wind values ($\lesssim$30 per cent differences), in spite of the causal contact between the neutron star and the stellar envelope. In addition, in all cases that we consider, the magnetar drives a collimated ($\sim$5–10°) relativistic jet out along the rotation axis of the star. Nearly all of the spin-down power of the neutron star escapes via this polar jet, rather than being transferred to the more spherical SN explosion. The properties of this relativistic jet and its expected late-time evolution in the magnetar model are broadly consistent with observations of long duration gamma-ray bursts (GRBs) and their associated broad-lined Type Ic SN.

Key words: magnetic field – MHD – stars: neutron – stars: supernovae: general – stars: winds, outflows – gamma-rays: bursts.

1 INTRODUCTION

Observations of long-duration gamma-ray bursts (LGRBs) have demonstrated that they are associated with core-collapse supernovae (SNe) and the death of massive stars (Della Valle 2006; Woosley & Bloom 2006; Zhang 2007). Two leading candidates for the central engine powering LGRBs are a newly formed, rapidly rotating magnetar (e.g. Usov 1992; Thompson 1994; Wheeler et al. 2000; Thompson, Chang & Quataert 2004) or a black hole with an accretion disc (e.g. MacFadyen & Woosley 1999). In both of these cases, it is crucial to understand how relativistic material generated by the central engine – which is believed to give rise to the GRB at large distances from the compact object – escapes from

deep within the host star. The most likely possibility, suggested by both afterglow observations ('jet breaks'; Rhoads 1999) and GRB energetics, is that a collimated outflow punches through the stellar envelope, providing a channel out of which the relativistic material can escape.

In the collapsar model, collimated outflows from GRBs are accounted for by jets produced by a centrifugally supported accretion flow on to a central black hole, based on the results of numerical simulations (e.g. Proga et al. 2003; Barkov & Komissarov 2008) and by analogy with X-ray binary and active galactic nucleus (AGN) jets.

In the magnetar model, however, the origin of such collimated outflows is less clear because relativistic outflows do not efficiently self-collimate (e.g. Lyubarsky & Eichler 2001). Numerical simulations of outflows from *isolated* magnetars have clearly shown that a highly collimated outflow can only be formed at very early times

⋆E-mail: nbucciantini@astro.berkeley.edu

(within a few seconds after core bounce) when the outflow is only mildly relativistic, while relativistic outflows can only be produced at later times when the latitudinal distribution of the energy-flux approaches that of the force–free solution, with most of the energy flux confined in the equatorial region and not along the axis (Bucciantini et al. 2006). These results appear to be independent of the specific magnetic field configuration on the surface of the star.

Energy considerations demonstrate, however, that the surrounding stellar envelope provides an efficient confining medium even for a very energetic proto-magnetar wind. Thus, the GRB outflow might be strongly affected by the interaction with the progenitor star (this is true in both the collapsar and magnetar contexts). Königl & Granot (2002) suggested, by analogy to pulsar wind nebulae (Begelman & Li 1992) (PWNe), that the interaction of the wind from the spinning-down magnetar with the surrounding star could facilitate collimation.

In two previous papers (Bucciantini et al. 2007, Paper I; Bucciantini et al. 2008, Paper II), we have investigated the dynamics of this interaction, using a variety of simplifying assumptions. In Paper I, we used axisymmetric thin shell calculations to demonstrate that collimation can indeed occur (see Uzdensky & MacFadyen 2006, 2007 for related ideas based on force–free rather than inertially loaded outflows). In Paper II, we used relativistic magnetohydrodynamic (MHD) simulations to investigate the interaction of a relativistic magnetized wind with the progenitor star, using winds with properties expected for proto-magnetars (based on Metzger, Thompson & Quataert 2007). By analogy with PWNe (Del Zanna, Amato & Bucciantini 2004; Komissarov & Lyubarsky 2004), we focused on the low-magnetization regime in which most (but not all) of the magnetic energy of the wind (associated with the toroidal component of the magnetic field) is assumed to be converted into bulk kinetic energy. We found that the magnetar wind shocks on the surrounding (exploding) stellar envelope, creating a bubble of relativistic plasma and magnetic field inside the star (a 'magnetar wind nebula'; MWN). Just as in PWNe, if the toroidal magnetic field in the bubble is sufficiently strong, the bubble expands primarily in the polar direction due to the 'tube of toothpaste' effect – the magnetic stress in the equator creates a total pressure gradient along the axis which is not balanced by any restoring force, thus driving the flow preferentially in the polar direction. The nebula itself is ultimately confined by the inertia of the SN ejecta, to which little energy is transferred, in contrast to the pressure confinement in traditional magnetic tower models (Sherwin & Lynden-Bell 2007) or confinement by a pressurized cocoon inside the progenitor star (Uzdensky & MacFadyen 2006). This distinction is largely dynamical. In traditional magnetic tower models, the exterior pressure is high enough to create a stationary contact discontinuity separating the jet matter from the stellar material. In our case, the contact discontinuity is typically out of equilibrium because the pressure in the interior is higher than that in the surrounding star; however, the stellar density is so high that the contact discontinuity moves at a very slow speed, much less than the sound speed in the interior of the bubble.

The results of Papers I and II, despite being obtained with different approaches (thin-shell semi-analytic calculations versus full relativistic MHD simulations) and utilizing different assumptions, demonstrate qualitatively similar overall dynamics. In both cases, however, in order to reduce the computational time of the calculations, the properties of the outflow from the central source were specified using a fixed prescription, based on previous results for free-flowing winds (Bucciantini et al. 2006; Metzger et al. 2007), and using superfast magnetosonic injection. One concern with this approach is that, if the termination shock (TS) between the wind and the surrounding star moves within the slow, Alfvén, or fast critical surfaces, the stellar envelope is causally connected to the central star, which may modify how the star spins down and loses rotational energy and angular momentum (invalidating the boundary conditions used at the central source). In order to properly address these issues, it is necessary to follow the dynamics from the proto-magnetar atmosphere out to large radii.

Komissarov & Barkov (2007) carried out such a simulation and found that there is indeed some causal contact between the stellar envelope and the central star. In spite of this difference relative to our assumptions in Papers I and II, the collimation of the outflow by magnetic stresses was similar to what we have previously found. Komissarov & Barkov (2007)'s simulations were only for ∼200 ms after core bounce, however, and thus only apply to the early non-relativistic phase of magnetar spin-down, not to the late-time relativistic, and potentially GRB-producing, phase.

In this paper, we build on our previous work by carrying out time-dependent axisymmetric relativistic MHD simulations of the development of magnetar outflows and their propagation through a surrounding star. We follow the dynamics of the proto-magnetar wind into the late-time relativistic phase (for ∼10 s), and from the injection radius located at the proto-neutron star surface to a distance of a few progenitor stellar radii. Given the computational requirements of this problem, which extends over several orders of magnitude in radius, and which involves time-scales ranging from 10^{-7} s in the proto-neutron star atmosphere to ∼10 s for jet propagation through the host star, we have not carried out a detailed parameter study, but have instead limited our investigation to a few fiducial cases.

As in Paper II, we assume that an outgoing SN shock has already created a central evacuated cavity (see Section 2 for details) and that the host star is spherically symmetric. Hydrodynamic studies of neutrino driven winds after successful core-collapse SNe show that at small radii the density is such that a region can form where the wind blows (Thompson, Quataert & Burrows 2005; Scheck et al. 2006). We generally refer to such region as 'cavity' in analogy with the standard terminology used in wind nebulae to describe the region occupied by the wind, even if this does not necessarily imply either a lower density or a non-monotonically decreasing density profile. However, unlike in Paper II, we make no direct assumptions about the properties of the magnetar outflow. We only set the physical conditions at the proto-neutron star surface; specifically, the density, temperature and the radial component of the magnetic field are imposed there. A transonic flow self-consistently develops, with a speed increasing with radius. The wind magnetization $\sigma = \Omega^2 \Phi^2 / \dot{M}$ (where Ω is the rotation rate, Φ the open magnetic flux and $\dot{M}$ the mass loss rate) changes in time as the mass loss rate drops due to the changing temperature and density in the neutron star atmosphere (which change as a result of the decreasing neutrino flux during the neutron star's Kelvin–Helmholz phase). Given that the outflow is not injected with fixed properties, but is instead allowed to self-consistently develop, any feedback due to the interaction with the progenitor star is properly modelled. As a result (and unlike in Paper II), we do not assume that magnetic energy (associated with the toroidal component of the magnetic field) is converted into kinetic energy at large radii in the wind. On the contrary, the outflows simulated here are always reasonably highly magnetized, from the early time (≲ a few seconds) non-relativistic wind in which the magnetic energy is comparable to the kinetic energy at large radii to the late-time magnetically dominated relativistic outflow. It is, however, worth noting that our calculations

may not capture various instabilities [e.g. three-dimensional (3D) ones] that could dissipate magnetic energy, converting it into thermal energy and ultimately bulk kinetic energy; this limit of low σ is explored in Paper II.

The remainder of this paper is organized as follows. In Section 2, we describe our numerical methodology. We then describe the results of our calculations, including their implications for the collimation of magnetar outflows in LGRBs, the spin-down of the central neutron star and nucleosynthesis of shock-heated stellar material (Section 3). Finally, in Section 4, we summarize our results and their implications.

2 NUMERICAL SETUP

All of the simulations were performed using Eulerian Conservative High Order (ECHO), a shock-capturing central-scheme for general relativistic ideal MHD; see Del Zanna & Bucciantini (2002), Del Zanna, Bucciantini & Londrilo (2003) and Del Zanna et al. (2007) for a detailed description of the equations and numerical algorithms.

The interaction of the magnetar outflow with the surrounding SN progenitor is investigated by performing two-dimensional (2D) axisymmetric simulations on a spherical grid. The domain in θ is the first quadrant from $\theta = 0$ to $\pi/2$, with reflecting boundary conditions for v_θ, v_ϕ and the magnetic field components B_θ and B_ϕ at the polar axis to enforce axisymmetry, and similar boundary conditions in the equatorial plane. The grid is uniform in the θ direction with 100 cells. Given that we are studying a wide range of spatial scales, from the proto-magnetar atmosphere at $\sim 10^6$ cm to the outer edge of the star at $\sim 2 \times 10^{10}$ cm, we have selected a logarithmic spacing in radius with an inner boundary located at $r_{\rm min} = 1.5 \times 10^6$ cm and an outer boundary at $r_{\rm max} = 6.5 \times 10^{10}$ cm, and 100 cells per decade in radius. Zeroth order extrapolation is assumed at the outer boundary. The code is second order in both space and time, with a monotonized central limiter, chosen in order to resolve the large density jump between the lighter relativistic plasma inside the MWN, associated with the magnetar outflow, and the heavier stellar envelope (the density can increase by a factor of $\sim 10^4$). We use a Schwarzschild metric to account for the gravity of the central proto-neutron star, which must be included to properly drive a transonic wind from the neutron star surface. We do not include the self-gravity of the progenitor star; the typical dynamical time-scale for the progenitor is longer than the duration of our simulations and so the gravity of the progenitor can be neglected to first approximation.

Our previous results (Papers I and II) imply that it takes $\sim$5–10 s for the magnetar outflow to emerge from the progenitor surface and accelerate into the circumstellar medium. For this reason, we follow the evolution of the system for $\simeq 10$ s. Note that most of the times quoted in this paper are given in seconds *after core bounce*. Our simulations begin 1 s after core bounce, which is approximately the time it takes for the proto-neutron star to contract to its final radius $\simeq 15$ km and for the neutrino driven wind to develop inside the SN ejecta (Scheck et al. 2006). In order to evolve the dynamics in the neutron star atmosphere at 1.5×10^6 cm, the Courant–Friedrichs–Levy (CLF) time-step must be $\lesssim 3 \times 10^{-7}$ s. This highlights the fact that studying the evolution of the system for the desired duration of ~ 10 s is very time consuming. As a consequence, we have been forced to make several simplifications in our treatment of the microphysics. In particular, we use an ideal gas equation of state with an adiabatic index of 4/3, which is appropriate for both the relativistic magnetar outflow and for the radiation pressure dominated

shocks that result due to the interaction with the surrounding star; the validity of this assumption is checked in Section 3.4.

The effects of neutrino heating and cooling, which are responsible for driving the wind, are primarily confined to a very small region around the proto-neutron star (Thompson, Burrows & Meyer 2001; Metzger, Thompson & Quataert 2007). We approximate the effect of neutrino heating by including an isothermal layer at small radii near the inner boundary. At the inner radius, we fix the rotation rate Ω and the value of the radial magnetic field $B_{\rm r}$, and we assume perfect conductivity so that $E_\theta = E_\phi = 0$. The temperature, density, and radial extent of the isothermal layer have been adjusted to reproduce reasonably accurately the mass loss rate obtained in more sophisticated one-dimensional (1D) calculations that include a detailed treatment of the microphysics (Metzger et al. 2007), and to still guarantee numerical stability (decreasing the temperature leads to numerical instabilities, especially at high magnetization). We found that a reasonable choice was for an isothermal layer extending from the stellar surface to 3×10^6 cm with a pressure p such that $\rho c^2/p \simeq 100$ (i.e. a sound speed $c_{\rm s} \simeq 0.1\,c$). The density ρ decreases in time $\propto t^{-2.7}$ in order to reproduce the decline in mass loss rate for a free wind that is caused by the decreasing neutrino luminosity of the neutron star in the first 10 s after core bounce (Burrows & Lattimer 1986); the radial extent and the sound speed (set by $p/\rho c^2$) in the isothermal layer are independent of time. Given that the wind is magnetocentrifugally accelerated, the value of the thermal pressure does not affect its asymptotic dynamics (so long as the wind is cold) and the energy deposited in the isothermal layer is negligible with respect to the SN energy or the proto-magnetar spin-down energy.

The evolution of the magnetization σ, and the mass, energy and angular momentum loss rates for a free wind are shown in Fig. 8 (dashed line), discussed in Section 3. A comparison between the mass loss rates obtained using the isothermal layer approach described here with a 1D model including a full treatment of the neutrino physics (Metzger et al. 2007) is shown in Table 1 and in Fig. 8. The agreement is very good. Note also that the methodology adopted here produces the correct latitudinal variation in the mass loss rate (see Bucciantini et al. 2006), with magnetocentrifugal support enhancing the mass loss rate at the equator by a factor of ~ 100 relative to the pole for a neutron star with a millisecond rotation period. Although we have emphasized the comparison to free-wind calculations as a way of calibrating our simplified model, it is important to stress that our boundary conditions only specify the density, temperature and magnetic field in the neutron star's atmosphere; they do not specify the mass, angular momentum or energy loss rates, which are determined self-consistently by the wind's dynamics.

As in Papers I and II, we use the $35\,{\rm M}_\odot$ [zero-age main sequence (ZAMS)] model from Woosley, Heger & Weaver (2002) as our progenitor star. The outer surface of the progenitor is located at 2.5×10^{10} cm. We assume that the density outside the star falls off as r^{-2} as expected for a wind. We have previously verified that for the range of radii we simulate, our results are independent of the outer density profile (Paper II).

Our calculations assume that a successful SN shock *has already been initiated* by ~ 1 s after core bounce. In order to account for the effect of the SN shock propagating inside the progenitor, the region between 10^9 and 2×10^9 cm is given an initial outward velocity corresponding to a total kinetic energy 2×10^{51} erg, similar to that used in the 1D explosion calculations of Woosley & Weaver (1995). This corresponds to the SN shock moving at $\simeq 1.5 \times 10^4$ km s^{-1}. Hydrodynamic studies of neutrino driven winds after successful

Table 1. Comparison of the free-wind mass loss rates obtained using the isothermal layer approach described in Section 2, with the values obtained by solving the full neutrino-heated MHD wind problem (Metzger et al. 2007), both using a 1D monopole magnetic field. The cases with period $= \infty$ correspond to non-rotating neutron stars, and are indicative of polar outflows in our 2D simulations. Time is after core bounce and mass loss rate $\dot{M}$ is in $M_\odot$ s^{-1}.

Time (s)	Period (ms)	Magnetic field (G)	$\dot{M}$ (Metzger et al. 2007)	$\dot{M}$ (this paper)
1	∞	10^{15}	1.5×10^{-4}	1.6×10^{-4}
1	1	10^{15}	1.2×10^{-2}	1.6×10^{-2}
1	3	10^{15}	3.0×10^{-4}	4.0×10^{-4}
2	∞	10^{15}	3.0×10^{-5}	3.1×10^{-5}
2	1	10^{15}	2.4×10^{-3}	2.9×10^{-3}
8	1	10^{15}	9.3×10^{-5}	9.0×10^{-5}
1	1	10^{16}	1.5×10^{-2}	1.9×10^{-2}
2	1	10^{16}	2.6×10^{-3}	3.0×10^{-3}

core-collapse SNe show that as the SN shock expands inside the star a cavity is left at small radii, inside of which the wind blows (Thompson et al. 2005; Scheck et al. 2006). To approximate this, our initial condition includes a cavity inside the progenitor with a radius of 10^9 cm, which is roughly the size of the collapsing progenitor and the location of the SN shock 1 s after core bounce. The cavity is initially filled with low density plasma in hydrostatic equilibrium.

The initial conditions used in this paper for the size of the cavity into which the wind emerges, and its overall density, are motivated by existing calculations of successful SN explosions. In the hundreds of milliseconds after the formerly stalled SN shockwave attains positive velocities and begins propagating through the overlying progenitor, a neutrino-driven wind emerges from the proto-neutron star. Because the pressure behind the SN shock drops rapidly as the volume of the cavity increases, the wind quickly establishes a sonic point. This emergence of a proto-neutron star wind in the few hundred milliseconds after a successful explosion is discussed in detail in a number of papers (Burrows, Hayes & Fryxell 1995; Janka & Mueller 1995; Thompson et al. 2005; Scheck et al. 2006; Arcones, Janka & Scheck 2007; see, in particular, figs 9 and 11 of Thompson et al. 2005 and fig. 5 of Arcones et al. 2007). In our calculations, the density in the initial cavity is chosen to be low enough that the proto-magnetar wind can initially expand freely into the cavity, as is seen in the successful explosions described above. The initial conditions do not, however, determine whether the wind can expand freely at later times; this depends on the subsequent evolution, which is self-consistently calculated. Although the precise details of the shock evolution in the first ~ 1 s after the explosion will depend on the progenitor density structure and the SN explosion mechanism, existing calculations demonstrate that the formation of a low-density cavity into which a neutrino-driven wind emerges is a generic property of models that explode, even if the explosion is asymmetric and the wind emerges anisotropically because the proto-neutron star continues to accrete at some latitudes (Burrows et al. 2006; Scheck et al. 2006). The results of our calculations are not that sensitive to the precise details of the initial cavity and its density structure (see Section 3.2), because the magnetar wind quickly expands into the cavity left by the outgoing SN shock.

The boundary conditions used here remove many of the assumptions about the wind structure that were used in our previous papers, and allow the outflow to develop freely and self-consistently according to the physics of the interaction between the wind and the progenitor star. The magnetic field is assumed to be monopolar and to extend from the surface of the proto-neutron star into the

SN progenitor. This formally corresponds to assuming a large fossil magnetic field in the progenitor. We expect, however, that our results would be very similar if the field is generated in situ by a convective dynamo (Duncan & Thompson 1992). For example, outside the light cylinder ($\simeq 10^7$ cm for a millisecond rotator), the structure and properties of the wind depend only on the amount of open magnetic flux, and not on its structure in the closed magnetosphere, so that the monopole solution is reasonable. Moreover, even if the poloidal magnetic field threads the entire star, at 10^9 cm (the initial size of the SN ejecta) it is dynamically negligible, and is unable to exert any significant torque on the central compact object. For the typical values of σ in our simulations, the amount of open magnetic flux in the wind implies that the dipolar magnetic field is a factor of ~ 2 larger than the monopole values quoted here (Bucciantini et al. 2006).

To explore a few reasonable models for magnetar central engines of LGRBs, we consider three cases, motivated by previous work (e.g. Metzger et al. 2007): case A is a 1 ms rotator with a $B_r = 10^{15}$ G surface magnetic field; case B is a 1 ms rotator with $B_r = 3 \times 10^{15}$ G; and case C is a 3 ms rotator with $B_r = 10^{15}$ G. In all cases, the rotation rate is kept constant in time. After the fact, we can assess that this is a reasonable assumption for both cases A and C, in that only a modest fraction of the rotational energy is lost during the 10 s of our simulation (see Fig. 8, discussed below). For case B, however, keeping the rotation rate constant is not fully self-consistent, because of the higher energy loss rate. Case B is none the less a useful guide to the dynamics in the high σ, high spin-down power limit.

Relativistic MHD codes can have numerical difficulties at sufficiently large σ and/or B^2/ρ. In case C, we found that we were not able to lower the mass loss rate, and thus increase σ, at late times, but had to artificially limit σ to be ≤ 12; this is true even for the free wind. Despite the fact that the magnetization is lower than in cases A and B, case C was less numerically stable. We suspect that this is because the slower rotation rate in case C leads to a smaller mass loss rate and thus lower densities. This affects the stability of the free wind, in which B^2/ρ grows sufficiently large to cause numerical difficulties at large distances. In addition, in case C there are more complex interactions between the magnetar wind and the SN ejecta (see Section 3.2): the compression of the magnetic field at small radii leads to the formation of strong current sheets that the code fails to handle properly. This happens only at late times, and is due to the compression of the magnetic field close to the Alfvénic surface at $\sim 10^7$ cm, much smaller than the typical size of the MWN (see Fig. 7, discussed below).

3 RESULTS

We first describe the results of cases A and B, which are qualitatively similar. Case C has a significantly lower spin-down power, and has a somewhat different evolution; this will be discussed separately at the end.

3.1 Cases A and B: high spin-down power

We first provide an overview of the evolution of the system as a function of time. The density in the initial cavity left by the expanding SN shock is small enough that the wind from the proto-magnetar can easily sweep through the cavity in a time $\sim R_{\mathrm{cavity}}/V_{\mathrm{wind}} \sim 0.1$ s. As soon as the wind impacts the high-density ejecta, it is forced to slow down to a speed of the order of SN shock velocity ~ 0.03 c, in a strong TS. This shock leads to the formation of a hot magnetized subsonic bubble (the MWN) whose evolution depends on the magnetization of the wind and on the spin-down power of the proto-neutron star.

In a 1D monopolar geometry, it is well known that the TS can only exist for a long time at significant distances from the neutron star in the limit of a weakly magnetized wind (known as the σ limit in PWNe; see Kennel & Coroniti 1984). For $\sigma > V_{\mathrm{MWN}}/c$ (where V_{MWN} is the expansion speed of the MWN, set initially by the SN shock velocity in our problem), the shock collapses towards the neutron star on a time-scale of the order of a sound crossing time, due to the compression of the toroidal magnetic field. We have carried out 1D relativistic MHD simulations of magnetar spin-down inside a star and have verified that for proto-magnetars with rotation rates and surface magnetic field strengths comparable to those considered here (see Table 1), the TS indeed collapses back down to the neutron star after ~ 0.03 s. The resulting causal contact between the central neutron star and the surrounding progenitor causes the neutron star to spin-down significantly faster than is predicted by free wind calculations (e.g. Metzger et al. 2007).

The evolution is, however, significantly different in the multidimensional problem considered here. As the wind from the central neutron star inflates the MWN, two competing effects occur. On one hand, magnetic field gets progressively compressed inside the bubble, causing the TS to recede to smaller radii, as in the 1D case.

On the other hand, the high total pressure inside the MWN pushes out against the denser SN ejecta. For a magnetized wind, the total pressure along the rotation axis is significantly larger than at intermediate latitudes or the equator, for reasons that we discuss in detail in Papers I and II. This leads to a preferential expansion of the MWN in the polar direction and the formation of an elongated bubble. As a result, the σ limit is less severe in 2D than in 1D: the magnetic field is allowed to flow from the equatorial region to the polar region. For large spin-down power (cases A and B), the expansion of the MWN in the polar region is fast enough to relieve the compression of the magnetic field by allowing an escape channel along the axis. As a consequence, the TS moves towards the central neutron star at a slower speed than in 1D. Once the jet emerges from the central part of the star, the outflow through the polar channel compensates for the injection of the magnetic field, the build-up of toroidal field in the nebula saturates, and the TS stabilizes.

Fig. 1 shows the radial velocity (in units of c) at three different times for case A, all approximately 2 s after core bounce; the three times shown are within $\simeq 0.15$ s of each other. Initially, the TS is outside the fast surface at all latitudes and its shape is roughly spherical. As discussed in previous papers about PWNe (Del Zanna et al. 2004), the shape of the TS can be understood qualitatively in terms of total pressure balance between the wind and the nebula. Fig. 2 shows the toroidal magnetic energy distribution in the nebula while Fig. 3 shows the total pressure. At early times, the wind is moderately relativistic and is collimated in the polar direction; the ram pressure is thus higher along the axis than at the equator. The nebula also has a higher axial total pressure due to the compressed toroidal magnetic field (Begelman & Li 1992). These two effects roughly balance and as a result the TS is roughly spherical. However, at later times the proto-magnetar wind becomes progressively more magnetically dominated, due to the decreasing neutrino flux from the proto-neutron star and the associated drop in mass loss rate. The spin-down power thus becomes progressively more equatorial. At the same time, the compression of the toroidal magnetic field in the MWN tends to increase the total pressure anisotropy in the bubble. As a result, the TS becomes oblate and a cusp forms at the pole, as can be seen at the later times in Fig. 1. As soon as the polar cusp forms, the inclination of the TS causes the formation of vorticity in the post-shock region; this leads to the formation of large-scale
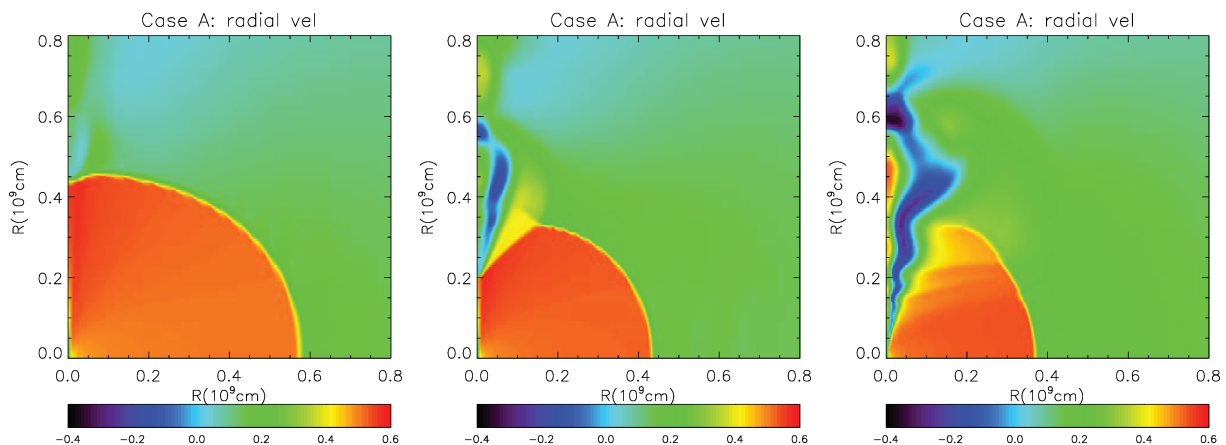

Figure 1. Evolution of the radial velocity (in units of c) in a magnetized bubble inflated by a magnetar with $B = 10^{15}$ G and $P = 1$ ms inside a 35 M$_\odot$ star (case A), about 2 s after core bounce (1 s after the start of the simulation). The time difference between the left- and right-hand panels is $\simeq 0.15$ s. During this time, the TS collapses to small radii, inside the fast surface, near the pole, but it remains well outside the fast surface at the equator; the fast surface is at $\simeq 6 \times 10^6$ cm at the equator and $\simeq 1.2 \times 10^8$ cm at the pole. Once the TS becomes significantly curved near the pole, turbulent eddies are created, as can be identified by the negative radial velocity; these are only moderately resolved in the current simulations.
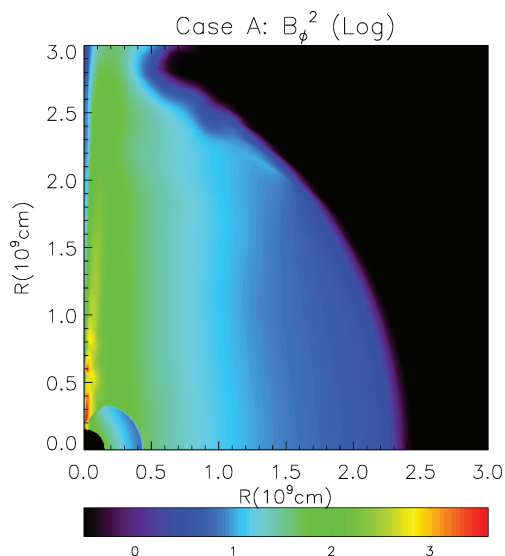
Case A: B_ϕ^2 (Log)

Figure 2. Azimuthal magnetic pressure ($\log_{10}[B_\phi^2/4\pi]$ (10^{21} erg cm^{-3})) for case A ≈ 2 s after core bounce. The magnetic energy is higher along the axis than near the equator. The central wind region has been excised to enhance contrast in the MWN.

eddies along the axis. Because of the angle between the wind and the shock, the cusp also strongly reduces the effective ram pressure exerted by the wind.

At later times, the TS along the axis moves to much smaller radii, inside the location of the fast surface (which along the axis is at a much larger distance from the neutron star than on the equator; e.g. Bucciantini et al. 2006). Once the TS reaches the fast surface, it becomes a weak Alfvénic discontinuity, and a subfast outflow is established in the polar region which puts the nebula in causal contact with the central engine (Fig. 1). However, in both cases A and B, the shock in the equatorial region never reaches the location of the fast surface for two reasons: first, the TS shock tends to be at larger radii in the equator because the total pressure in the nebula is lower at the equator than at the pole while for high σ the wind ram pressure is higher at the equator (see Del Zanna et al. 2004 for a detailed discussion of the shape of the TS); second, the fast surface is closer to the central engine in the equator ($\simeq 60$ km at the equator and $\simeq 10^8$ cm at the pole). The result is a mixed outflow in which the flow is subfast (but super-Alfvénic) in the polar region but superfast in the equatorial region. We will discuss the implications of this causal contact for the spin-down of the neutron star in Section 3.3.

In both cases A and B, the expansion in the polar region is fast enough that even at relatively early times, the MWN has already created a jet-like feature along the rotation axis that is expanding at speeds that are a reasonable fraction of the speed of light. Figs 3 and 4 show the later time evolution of the density, total pressure and velocity, for cases A and B, respectively. The polar jet expands much more rapidly than the SN shock and by ~ 3–5 s the jet is outside the surface of the progenitor star. Despite some quantitative differences, the late-time evolution of the MWN is quite similar to that found in Paper II, in which we injected a high γ, low σ wind.

As soon as the jet starts expanding into the lower density circumstellar region, it accelerates to high speeds. For computational reasons, we cannot follow the acceleration of the jet for more than a few stellar radii, and thus we cannot completely assess the asymptotic acceleration of the outflow. For the range of radii that we do study, we find that the Lorentz factor in the jet at late times is smaller

than the value of σ at the base of the proto-neutron star wind at the same time (the maximum achievable γ), but larger than the $\gamma \simeq \sigma^{1/3}$ acceleration of the 1D monopole. Specifically, in case A, we find a Lorentz factor $\gamma \sim 4$ near the axis of the jet when $\sigma \sim 10$ in the free wind at $t \simeq 10$ s; in case B, $\gamma \sim 10 - 15$ when $\sigma \sim 60$ (see the top panel in Fig. 5). The magnetization of the jet itself at large radii is also not negligible: in case A, the jet has a magnetic field that is close to equipartition $[B^2/\gamma^2(\rho c^2 + 4P)\beta_r \simeq 1]$, while in case B it is somewhat above equipartition $[B^2/\gamma^2(\rho c^2 + 4P)\beta_r \simeq 5]$. This largely accounts for the fact that the acceleration is not 100 per cent efficient. Indeed, the late-time magnetic + kinetic energy in the jet at large radii is comparable to the late-time value of the magnetic energy in the magnetar wind at small radii. This is a non-trivial result since the MWN tends to accumulate the flow so that the highly magnetized late-time outflow could have been partially mixed with the earlier less magnetized outflow.

Although the magnetar wind efficiently and rapidly creates a collimated polar jet that allows relativistic material to escape the host star, the overall interaction with the relatively spherical SN ejecta is much weaker; in particular, little of the magnetar spin-down power is transferred to the spherical SN ejecta. This is true even at late times when the energy flux in the free magnetar wind at small radii is largely equatorial. The reason is that the wind undergoes a TS and then escapes via the polar channel. The low equatorial total pressure in the MWN leads to very little energy transfer to the ejecta near the equator. In case A, we do find that the MWN is able to partially compress the shocked SN ejecta in the first few seconds, but as soon as the jet develops the internal energy of the MWN escapes via the polar channel and the SN ejecta start to recede inside and partially recompress the MWN. However, in neither case A nor case B do we find any significant changes in the global properties of the SN shock inside the progenitor star due to the magnetar wind.

To quantify this, Fig. 5 shows, for cases A and B, the relation between the instantaneous power in the magnetar wind at small radii, the energy flux in the relativistic core of the jet at large radii (defined to be the energy flux within $5°$ of the pole) and the energy flux in the wider angle wind at large radii (defined to be the energy flux within $20°$ of the pole). Fig. 5 demonstrates that essentially all of the energy injected by the central engine is carried away in the collimated jet with a significant fraction of the energy confined in the central relativistic core. Note that there are ~ 10–20 per cent fluctuations in the energy flux due to turbulence created in the curved TS near the axis; there are significant fluctuations in the Lorentz factor as well (top panel). It is also interesting to note that the energy flux in the jet and wind at large radii is on average a little higher than the energy flux in the wind at small radii at the same time. This is because energy injected by the wind at earlier times can be stored in the MWN, and released later on. The MWN thus introduces a small delay between conditions in the wind at injection and conditions in the jet emerging from the star.

The vorticity created at the curved TS in the polar region leads to the development of a layer where sausage modes grow unstable. It is reasonable to expect that in a more realistic (e.g. 3D) calculation, these instabilities might lead to the dissipation of some of the toroidal field. In Section 4, we will discuss how these instabilities might modify the evolution of the system.

3.2 Case C: lower spin-down power

We now discuss case C, which corresponds to a magnetar with $P = 3$ ms and $B = 10^{15}$ G (see Fig. 6). This case differs from the
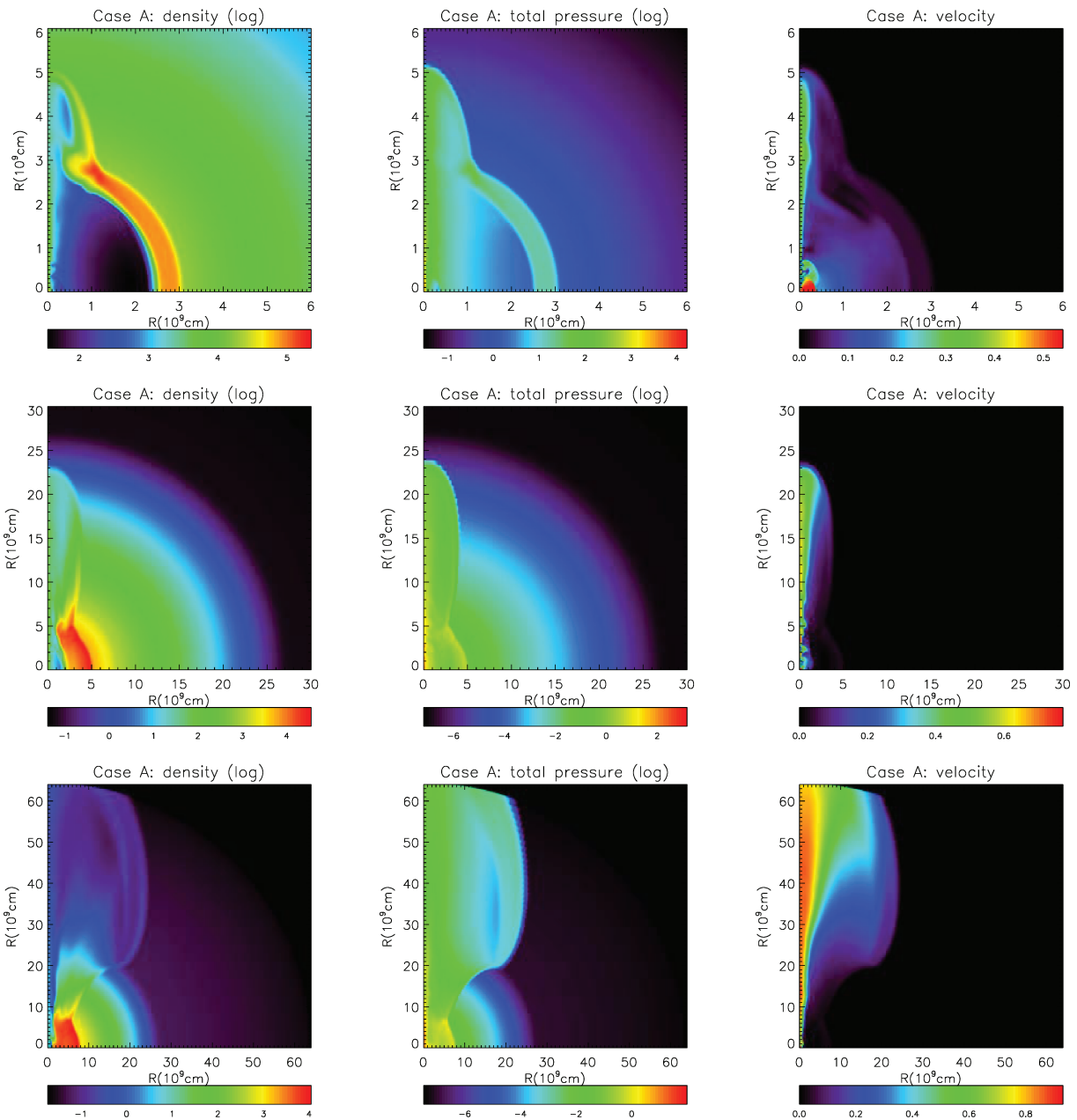
Figure 3. Evolution of the magnetized bubble inflated by a magnetar with $B = 10^{15}$ G and $P = 1$ ms inside a $35\,M_\odot$ star (case A). From left to right, the panels show: $\log_{10}$[density (g cm^{-3})], $\log_{10}$ [total pressure (erg cm^{-3} c^2)] and velocity (in units of c). From top to bottom, the snapshots are 2, 4 and 7 s after core bounce. The radius of the progenitor star is 2.5×10^{10} cm. By $t \sim 5$ s (middle panel) the jet has escaped the progenitor star.

previous two in two important ways: first, the typical spin-down power is a factor of $\sim$10 ($\sim$100) lower than in case A (case B); and, second, the location of the light cylinder and thus the fast surface is at a larger distance. Because of the lower spin-down power, the evolution of the MWN proceeds more slowly than in cases A and B. 10 s after the launching of the wind, the MWN has barely emerged from the progenitor star.

The evolution of the MWN is also qualitatively different from the higher spin-down power cases. The lower net pressure in the MWN implies that the nebula expands at a significantly slower speed. As a result, even though the total pressure along the rotation axis is larger than that at the equator, the expansion of the polar jet is not fast enough to overcome the compression of the toroidal field in the nebula, and so the TS collapses to smaller radii

(unlike in the higher spin-down cases where the rapid polar expansion allows the system to avoid this fate). A subfast flow is first established in the polar region, but after about 1 s the TS contracts within the fast surface along the equator as well, resulting in a fully subfast outflow. The dynamics in this case is qualitatively similar to that found by Komissarov & Barkov (2007) although the absolute radial scales are larger. In Section 3.3, we will discuss the implications of the subfast outflow for the spin-down of the proto-magnetar. As in the previous cases, vorticity is created downstream of the TS that generates turbulence which persists to late times. This turbulence gives rise to significant interpenetration of the wind and the SN ejecta, in the form of fingers of SN ejecta that are dragged down to small radii, as is shown in the zoom-in to small radii in Fig. 7. At late times, the denser SN ejecta
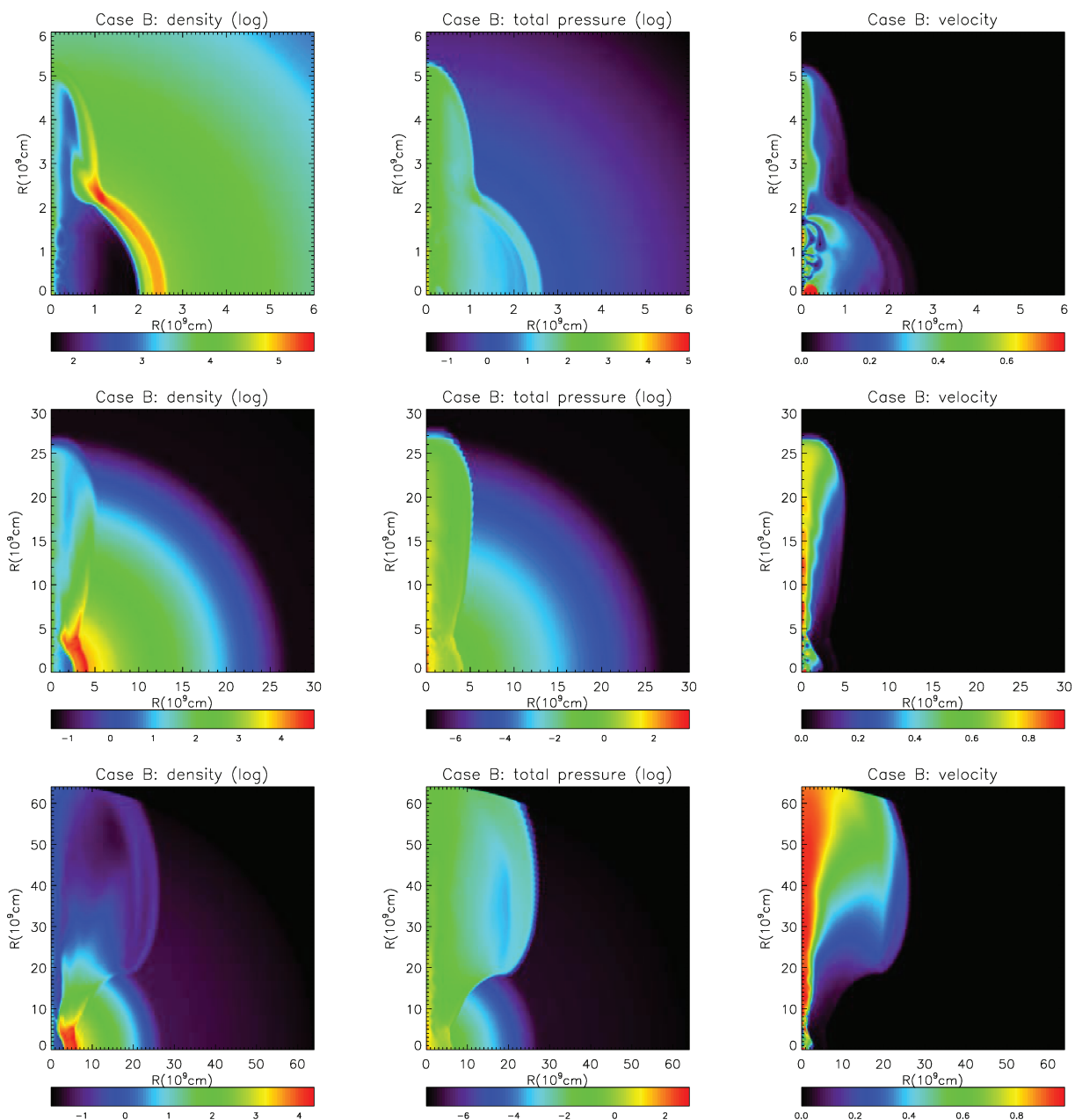
Figure 4. Evolution of the magnetized bubble inflated by a magnetar with $B = 3 \times 10^{15}$ G and $P = 1$ ms inside a 35 M$_\odot$ star (case B). From left to right, the panels show: $\log_{10}$[density (g cm^{-3})], $\log_{10}$[total pressure (erg cm^{-3} c^2)] and velocity (in units of c). From top to bottom, the snapshots are 1.6, 3, and 5 s after core bounce. The radius of the progenitor star is 2.5×10^{10} cm. By $t \sim 3$ s (middle panel) the jet has escaped the progenitor star.

even compress the magnetar wind at radii close to the Alfvénic surface.

We have attributed the differences between cases A/B and case C – namely a largely superfast versus fully subfast outflow – to the differences in spin-down power and rotation rate. One concern might be whether these properties of the outflow are sensitive to the size of the 'SN' cavity we initialize. To assess this, we have repeated case A using a cavity with an initial radius of 5×10^8 cm, a factor of 2 smaller than in our fiducial case shown in Fig. 3. At very early times $\lesssim 1$ s, the smaller cavity does modify the solution, leading to a fully subfast outflow because the TS is at smaller radii. However, as the system evolves and the MWN expands into the outgoing SN ejecta, a superfast outflow is again established in the equatorial region. After ~ 1 s, the system relaxes to a configuration

similar to that which we found starting with a larger initial cavity. This demonstrates that the primary physics determining whether the magnetar wind is superfast or subfast is indeed the spin-down power of the neutron star.

3.3 Proto-neutron star spin-down rate

In all of our simulations, there is at least some fraction of the proto-neutron star outflow that is in causal contact with the surrounding stellar envelope. In the higher spin-down power simulations (cases A and B), the polar region is subfast, while in the lower spin-down power simulation (case C), the entire outflow is subfast. In all three cases, the outflow is always super-Alfvénic. Because of this causal contact, it is possible that the spin-down of the neutron
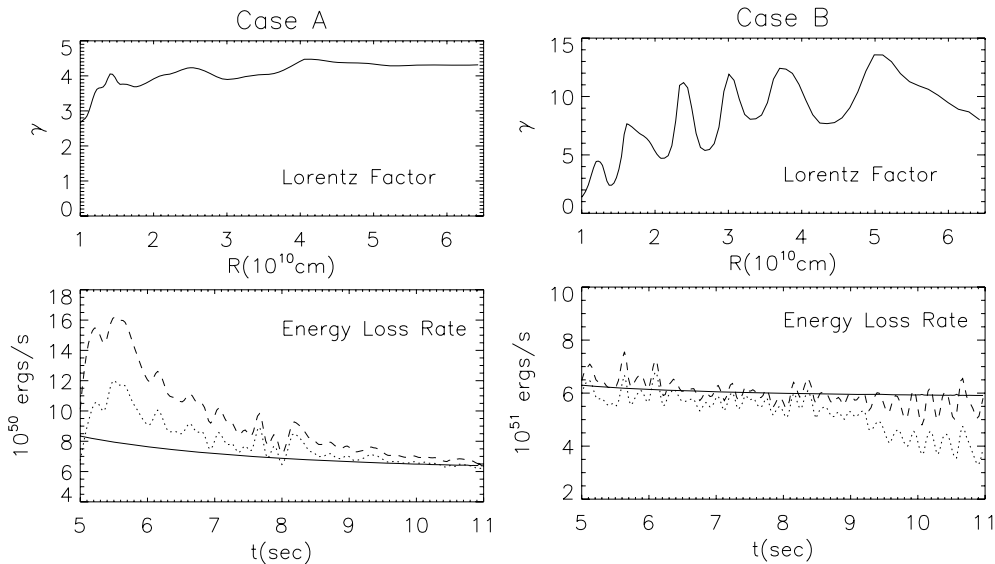
Figure 5. Outflow and spin-down properties for cases A (left) and B (right). Upper panels: Lorentz factor in the jet along the axis as a function of radius, at the end of the simulation ($t = 11$ s after core bounce). Lower panels: comparison of the energy flux in the magnetar wind at small radii near the neutron star (solid line), energy flux in the jet at large radii (dotted) and energy flux in the cocoon at large radii (dashed). The jet is defined to be within 5° of the axis, while the cocoon is within 20° from the axis.

star could be modified from that due to a free wind. Understanding the torque on the central engine is important because it strongly influences whether or not conditions suitable for producing GRBs can be achieved. For example, an increased torque due to a subfast outflow might lead to sufficiently rapid spin-down that most of the rotational energy has been depleted before the outflow becomes relativistic.

Fig. 8 shows the magnetization, mass loss rate, energy loss rate and angular momentum loss rate for the central neutron star in our simulations (solid) compared to the corresponding results for free winds (dashed lines). Fig. 8 shows that for cases A and B, the energy and angular momentum losses in the wind are essentially identical to those of a free wind. At first, this seems to contradict the fact that a subfast wind has a larger torque than a superfast wind in 1D calculations. However, for cases A and B, the subfast outflow is present only in the polar region, while at high σ most of the torque is exerted by the equatorial outflow. The polar outflow thus makes only a small contribution to the total torque even if it causally connected with the envelope.

The close similarity between the torque in our simulations and that exerted by a free wind can also be understood in terms of the location of the critical surfaces. In 1D, there are two free parameters at the inner boundary (i.e. B_ϕ and v_r) and two corresponding critical points, the slow and fast magnetosonic points; the equations can be renormalized to eliminate the singularity at the Alfvén point, which is automatically crossed once the solution passes smoothly through the slow and fast points. These two critical points correspond to two eigenvalues of the system: the mass loss rate, associated with the slow point, and the terminal Lorenz factor, associated with the fast point (the torque, which is also an eigenvalue, is determined by the Alfvén point, and, in 1D, is fixed once the other two are known). In 2D, however, there are three free parameters at the inner boundary (B_θ, in addition to v_r and B_ϕ) and three corresponding critical surfaces and three independent eigenvalues: the slow, fast and Alfvén surfaces. In order to modify the torque significantly, the location and shape of the Alfvén surface must be modified. For fast rotators like those considered here, this implies that the outflow

must be modified inside the light cylinder. We find, however, that even if the TS moves inside the fast surface, the location of the Alfvén surface remains relatively unchanged.

The results for case C – in which the outflow is fully subfast – are somewhat different than those for cases A/B. Although the torque and energy losses are nearly identical to that of the free wind at early times, at late times the energy losses tend to be more variable and can be ~30 per cent higher than for the free wind (Fig. 8). These large fluctuations correspond to when the post-TS turbulence is able to compress the proto-magnetar wind down to radii that are close to the light cylinder (Fig. 7). This level of fluctuations, while interesting from the point of view of the underlying physics of the problem, is unlikely to change the overall evolution of the system in a significant way.

3.4 Post-shock nucleosynthesis

Our calculations have assumed an ideal gas equation of state with an adiabatic index of 4/3, which is appropriate for a radiation dominated flow or for relativistic conditions. We have checked a posteriori that this assumed adiabatic index is consistent with the thermal properties of the MWN and jet. Fig. 9 shows the temperature derived from inverting the relation

$$p = \frac{k_B \rho T}{\mu m_p} + \frac{aT^4}{3} \qquad (1)$$

between the total pressure and density in our simulations, at $t = 1.6$ s after core bounce. At almost all locations, the temperatures are high enough that the radiation pressure dominates and thus our equation of state is self-consistent.

The temperature of the gas is also important for understanding nucleosynthesis during the SN explosion. For example, explosive nucleosynthesis of ^{56}Ni requires temperatures of $\gtrsim 5 \times 10^9$ K (Woosley et al. 2002). Fig. 9 shows that this temperature is not attained even at relatively early times in our simulations. The reason for this is the low density of the outer stellar envelope. By the
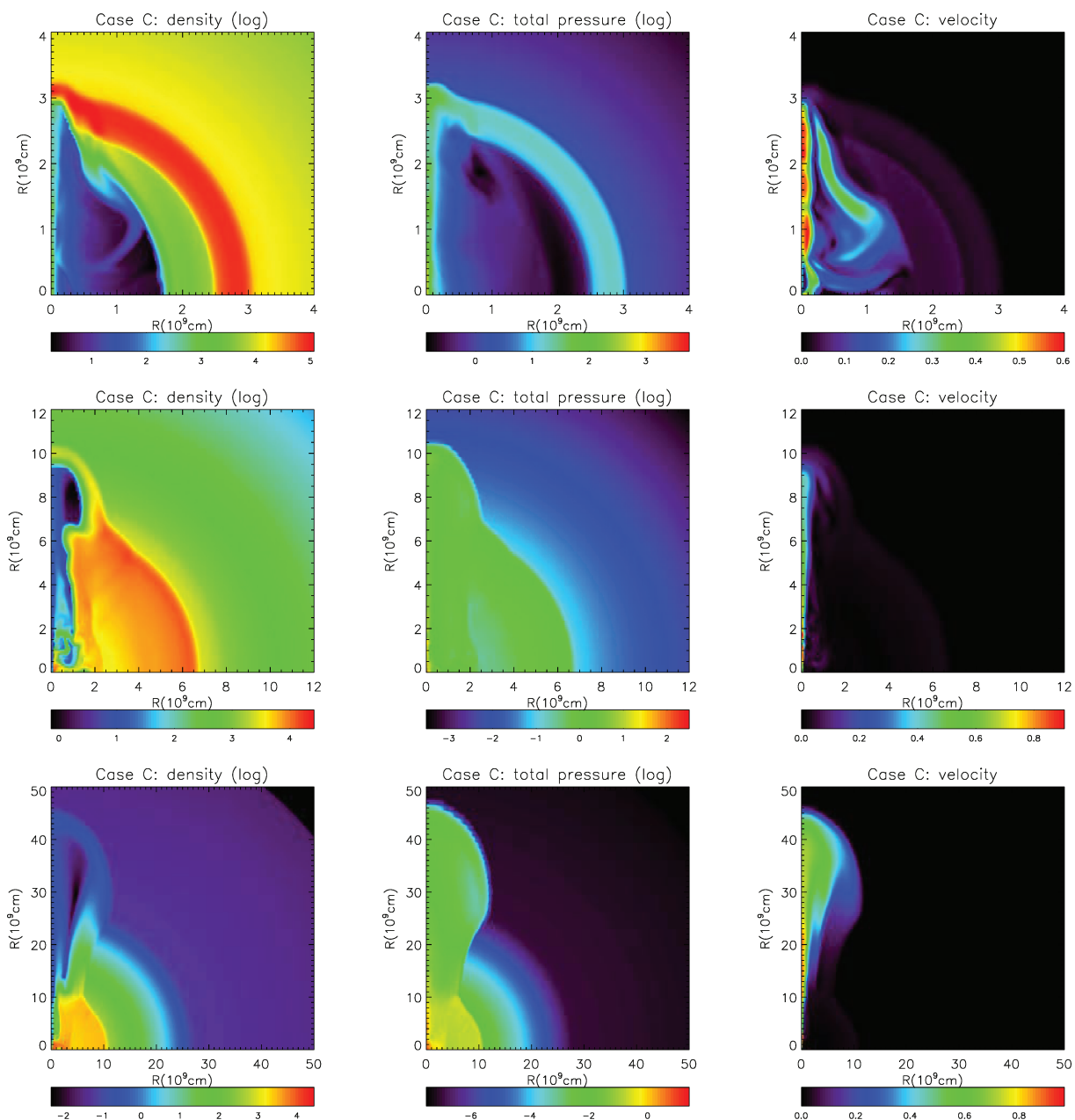
Figure 6. Evolution of the magnetized bubble inflated by a magnetar with $B = 10^{15}$ G and $P = 3$ ms inside a 35 $M_\odot$ star (case C). From left to right, the panels show: $\log_{10}$[density (g cm^{-3})], $\log_{10}$[total pressure (erg cm^{-3} c^2)] and velocity (in units of c). From top to bottom, the snapshots are 2, 6 and 11 s after core bounce. Distances are in units of 10^9 cm; the radius of the progenitor star is 2.5×10^{10} cm. By $t \sim 10$ s (bottom panel) the jet has just started to escape the progenitor star.

time the jet-plume emerges outside the SN shock, the density of the progenitor is $\sim 10^{4-5}$ g cm^{-3}. At these densities, Ni production requires a shock moving at nearly the speed of light, significantly faster than what we find even for our most energetic explosion (case B). We do find, however, that $\sim 10^{-2}$ $M_\odot$ of high speed ($v \simeq 0.1$–0.2 c) Ne and O can be created, because these have lower threshold temperatures for successful explosive nucleosynthesis. The synthesized mass is relatively low because only a small solid angle near the pole is shock heated to sufficiently high temperatures by the jet. In the context of observed GRBs, our viewing angle is relatively *on-axis*, in which case the high velocity nucleosynthesis may be observable; high-velocity O and Ne can also be produced by the jet

blowing out stellar material that had been processed during stellar evolution (Mazzali et al. 2006). Even if the jet nucleosynthesis only contributes marginally to the total nucleosynthesis during the explosion, it might lead to unique observable signatures in the ejecta at late times (as may be the case for Cas A; Wheeler, Maund & Couch 2008).

It is clear that the jet could interact with higher density gas, and thus be more likely to produce Ni, at early times $\lesssim 1$ s, when the SN shock and MWN are smaller. However, the physics at these early times is uncertain: the magnetar is likely still contracting to its final radius and the magnetic field may even still be growing via a dynamo. Moreover, the early time evolution is likely to be
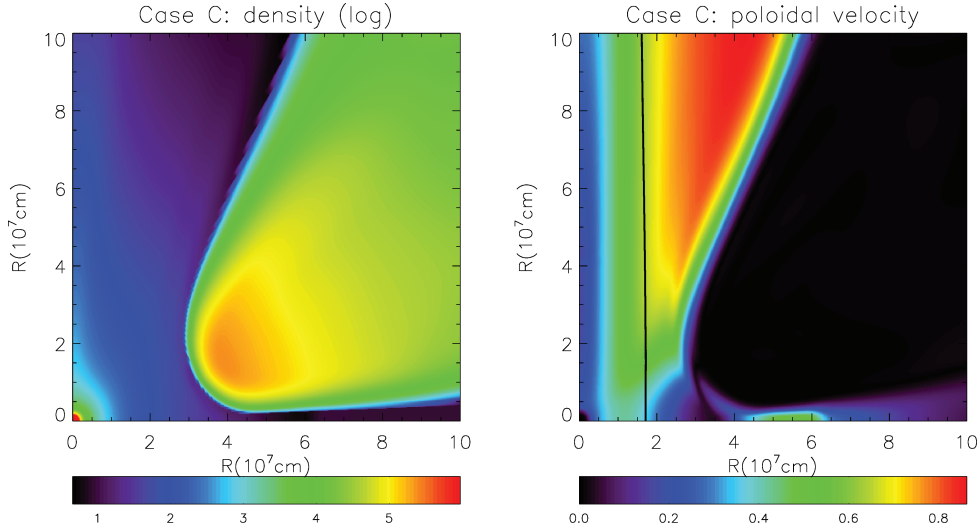
Figure 7. Density (left-hand panel) and poloidal velocity (in units of c; right-hand panel) in the inner 10^8 cm near the end of our simulation of case C ($B = 10^{15}$ G and $P = 3$ ms). The vertical solid line near a cylindrical radius of 170 km in the velocity plot is the location of the Alfvén surface. Note that the dense and slow moving stellar ejecta has compressed and redirected the magnetar's wind almost down to the Alfvén surface. This leads to the enhanced torque and larger spin-down variability seen in Fig. 8
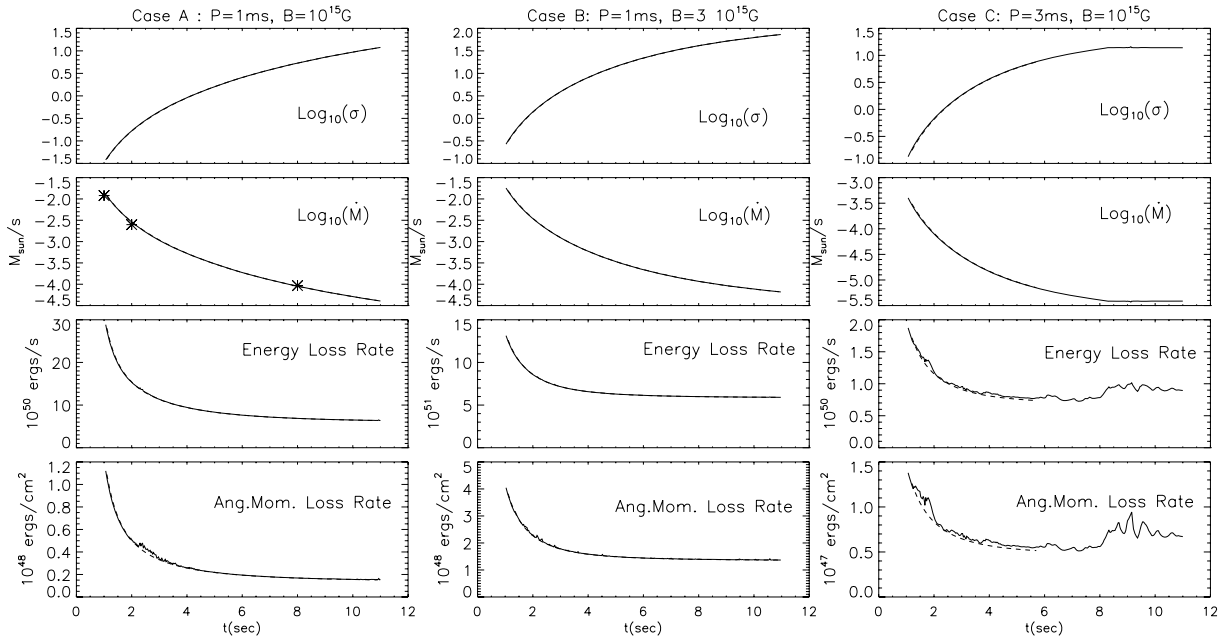
Figure 8. Magnetization σ and mass, angular momentum and energy losses for cases A (left), B (centre) and C (right). The dashed line represents the same quantities computed for the free wind; for case C, the free wind was numerically unstable at late times and so is not plotted after $\simeq 6$ s (Section 2). For case A, we also show the mass loss rate at three times (stars) from the calculations of Metzger et al. (2007), who included realistic neutrino microphysics.

more sensitive to the details of the explosion mechanism. As described previously (Section 3.3), we have verified that the late-time spin-down of the proto-neutron star and the formation of the collimated jet are not sensitive to the size of the initial cavity we choose (which is a proxy for the uncertain SN physics). This will not be true of the amount of Ni synthesized. We thus conclude that a more careful treatment of the early time contraction and spin-down of the magnetar, probably together with a better understanding of the SN mechanism, are required to reliably assess the question of whether the central engine responsible for the GRB also contributes significantly to the production of Ni during long-duration bursts.

4 DISCUSSION AND IMPLICATIONS

The calculations presented in this paper, together with our previous work (Papers I and II), show that the production of a collimated relativistic jet that can escape the progenitor star is a robust consequence of the formation of a $B \sim 10^{15}$ G, $P \sim 1$ ms neutron star during core-collapse SNe. Paper II shows that such a jet is formed in the low σ limit in which most of the magnetic energy in the magnetar's outflow has been converted into bulk kinetic energy – a limit motivated by observations of PWNe which show that such efficient conversion takes place (e.g. Kennel & Coroniti 1984). In this paper, we have focused on the opposite limit, that of a highly
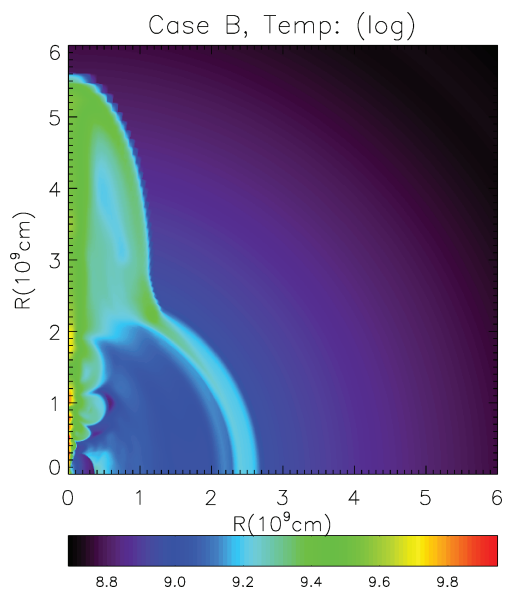
Figure 9. Temperature ($\log_{10}[T\ (K)]$) for case B at $t = 1.6$ s after core bounce. The temperature is never high enough for significant nucleosynthesis of ^{56}Ni, which requires $T \gtrsim 5 \times 10^9$ K, but some nucleosynthesis of carbon and oxygen will occur in material shock heated by the polar jet.

magnetized outflow in which the only conversion of magnetic energy into kinetic energy is that which takes place in ideal MHD. Just as in the low σ limit, we find that a bipolar jet begins to form in the first $\sim$1 s after core-collapse and escapes the star after $\sim$3–10 s (depending on the exact values of B and P; see Figs 3–6). Given the uncertainties in the conversion of magnetic energy into kinetic energy in magnetized outflows, it is reassuring that the properties of the GRB-producing jet are *not* that sensitive to these details. Physically, this is because in all cases the toroidal magnetic field produced by the central neutron star builds up in the cavity created by the outgoing SN shock (let us recall here that by 'cavity' we intend the region where the wind blows and not necessarily a lower density region or a non-monotonic density profile), until the field is sufficiently strong to drive the flow out in the polar direction; because the speed of the SN shock $\sim$0.03 $-$ 0.1 c is much less than the speed of the magnetar wind $\sim$ c, such a build up of toroidal field is inevitable unless the magnetic energy in the wind is extremely small ($\sigma \ll 0.01$).

An important result of our work is that nearly all of the spin-down energy of the neutron star escapes via the polar channel (Fig. 8). There is very little energy transferred to the exploding star in the equatorial region. We again find this in both the low (Paper II) and high (this paper) σ limits. One implication of this result is that the central engine powering the GRB is unlikely to contribute significantly to energizing the SN shock as a whole (although it clearly does so in the polar region), at least on time-scales $\gtrsim$1 s after core bounce; at earlier times, the dynamics will be sensitive to the details of the SN mechanism. We believe that this conclusion is not specific to the particular central engine considered here, but will hold for all *magnetically driven* GRB central engines. Specifically, we suspect that wide-angle magnetized winds from accretion discs, such as are seen in simulations of accretion discs relevant to GRBs (e.g. Proga et al. 2003), will form a magnetized bubble that will escape via the polar channel rather than transferring energy to the SN shock as has been previously hypothesized (Arons 2003; Kohri, Narayan & Piran 2005).

Observationally, there is a strong association of long-duration GRBs with core-collapse SN, in particular energetic SN Ic-BL (broad line) (Della Valle 2006; Woosley & Bloom 2006). However, the converse is not true (Soderberg et al. 2006; Woosley & Bloom 2006). Late-time radio observations of large samples of Type Ibc SN find that even the broad-line subset do not show evidence for an energetic relativistic outflow, which would produce radio emission at late times regardless of whether or not any putative gamma-ray emission was initially beamed towards us (Soderberg et al. 2006). More concretely, Soderberg et al. (2006) rule out with 84 per cent confidence the hypothesis that every broad-lined SN harbours a GRB. Moreover, the SNe associated with long-duration GRBs are not particularly unusual among the class of BL SN in terms of their energies, photospheric velocities and Ni masses (e.g. Soderberg 2006; Woosley & Bloom 2006). A plausible interpretation of these data is that some not yet fully understood physics (rotation?) leads to a class of core-collapse SNe that is unusually energetic and asymmetric (as revealed by spectra polarimetry), and that produce significant amounts of Ni. A subset of those SNe in turn produce relativistic jets that power GRBs, but the central engine that powers the GRB does not significantly modify the global properties of the coincident SNe. Clearly, the detection of a GRB implies a preferential viewing geometry along the rotation axis of the system; this is likely accompanied by the detection of a modest amount of high-velocity ejecta and nucleosynthetic products (Section 3.4). However, there is no indication that the global properties or the off-axis appearance of the SNe associated with GRBs are strongly affected by the central engine that produces the relativistic jet. Indeed, our results demonstrate that after $\simeq$1 s, most of the energy produced by a spinning-down magnetar escapes along the polar jet rather than energizing the SN shock. As argued above, we suspect that this result is likely to hold for all magnetically driven GRB models, including accretion discs on to black holes, but this remains to be explicitly demonstrated.

In our calculations, we have assumed that the ideal MHD holds in the magnetized bubble created behind the SN shock. It is, however, well known that plasmas with a primarily toroidal magnetic field can be unstable to non-axisymmetric kink modes (Begelman 1998) that would not be captured by our axisymmetric simulations (although such instabilities may be stabilized by rotation; see Tomimatsu, Matsuoka & Takahashi 2001). This raises obvious questions about the overall stability of the magnetic configuration found here (see also the recent results by McKinney & Blandford 2009 about jet stability). Unfortunately, it is not presently feasible to carry out 3D simulations of our magnetar wind model with the necessary spatial resolution and temporal duration. As noted above, however, the production of a relativistic jet by the interaction of a magnetar wind with the surrounding stellar envelope appears to be relatively insensitive to the precise magnetization of the outflow – as a comparison of the results of this paper and those of Paper II demonstrates. The most significant difference is in the acceleration of the jet once it emerges from the progenitor star: in the highly dissipative case (Paper II), the terminal Lorentz factor is larger ($\sim\sigma$ at the Light Cylinder), while in ideal MHD (this paper), the terminal Lorentz factor is somewhat lower, but the outflow remains reasonably strongly magnetized ($\sigma \gtrsim 1$) at the radii we can study. We thus conclude that unresolved instabilities are unlikely to change the large-scale evolution of the magnetar wind bubble or the resulting production of a collimated jet, but they may well be important in determining the acceleration of the jet and the exact ratio of magnetic to kinetic energy in the jet at large radii.

Our results also have implications for the nucleosynthesis of heavy elements due to the interaction between the magnetar-driven jet and the stellar envelope; we largely confirm previous studies on nucleosynthesis in jets and asymmetric SNe, which were based on parametrized models for the origin of the jet/asymmetry (Maeda et al. 2002; Nagataki et al. 2003; Nagataki, Mizuta & Sato 2006). As noted above, most of the energy produced by the magnetar is diverted into a jet with an opening angle of ~ 5–$10°$. The amount of mass swept up by the jet is $\sim 0.1\,M_\odot$, most of which is oxygen in the stellar model we use (Woosley et al. 2002). Even in our most energetic simulations, the temperature at the head of the jet is insufficient to produce ^{56}Ni (Section 3.4 and Fig. 9). It is, however, sufficient to produce $\sim 10^{-2}\,M_\odot$ of high-velocity Ne and Mg, and perhaps a similar amount of high velocity oxygen. Unfortunately, the high-velocity oxygen that is observed in some SNe associated with GRBs (Mazzali et al. 2006) can easily be explained as part of the stellar envelope that is blown out by the jet, and thus these observations do not strongly constrain the properties of the material shock heated by the head of the jet as it propagates through the star. The reason that our calculations do not produce a significant amount of ^{56}Ni is that we initialize our simulations roughly 1 s after core bounce, at which time the SN shock has moved to $\sim 10^9$ cm and the post-shock temperature at the head of the jet is $\lesssim 5 \times 10^9$ K. The temperature could be higher at earlier times, but the physics at earlier times, and the amount of ^{56}Ni produced, will likely depend sensitively on the physics of the SN explosion itself.

Our simulations span a factor of ~ 100 in the neutron star's spin-down power (Fig. 8). In our high spin-down power simulations, corresponding to neutron stars with $P = 1$ ms and $B \sim 1$–3×10^{15} G, we find that the outflow remains largely out of causal contact with the surrounding stellar envelope. In particular, unlike in 1D models of highly magnetized outflows (Kennel & Coroniti 1984), in our 2D calculations we find that even for high σ, the TS between the superfast magnetosonic wind and the hot shocked magnetar wind bubble lies outside the wind's fast magnetosonic surface, except very near the pole (Fig. 1). Physically, this is because the toroidal magnetic field can escape via the polar jet before it accumulates sufficiently in the magnetar wind bubble to drive the TS to small radii (as occurs in 1D). As a result, the spin-down of the neutron star is essentially identical to that of a free wind, i.e. a wind without a surrounding stellar envelope (Fig. 8). For our lowest spin-down power simulation, corresponding to a 3 ms rotator, the TS does collapse inside the fast magnetosonic surface (as Komissarov & Barkov 2007 found in their 2D simulations). Even in this case, however, the neutron star's spin-down is still quite similar to that produced by a free wind, with at most ~ 30 per cent differences (Fig. 8). In practice, these results imply that free wind calculations (e.g. Metzger et al. 2007) can be usefully used to study the winds from newly formed magnetars.

ACKNOWLEDGMENTS

REFERENCES

Arcones A., Janka H.-T., Scheck L., 2007, A&A, 467, 1227
Arons J., 2003, ApJ, 589, 871
Barkov M. V., Komissarov S. S., 2008, MNRAS, 385, L28
Begelman M. C., 1998, ApJ, 493, 291
Begelman M. C., Li Z., 1992, ApJ, 397, 187
Bucciantini N., Thompson T. A., Arons J., Quataert E., Del Zanna L., 2006, MNRAS, 368, 1717
Bucciantini N., Quataert E., Arons J., Metzger B. D., Thompson T. A., 2007, MNRAS, 380, 1541
Bucciantini N., Quataert E., Arons J., Metzger B. D., Thompson T. A., 2008, MNRAS, 383, L25
Burrows A., Lattimer J. M., 1986, ApJ, 307, 178
Burrows A., Hayes J., Fryxell B. A., 1995, ApJ, 450, 830
Burrows A., Livne E., Dessart L., Ott C. D., Murphy J., 2006, ApJ, 640, 878
Della Valle M., 2006, Chin. J Astron. Astrophys. Suppl., 6, 010000
Del Zanna L., Bucciantini N., 2002, A&A, 390, 1177
Del Zanna L., Bucciantini N., Londrilo P., 2003, A&A, 400, 397
Del Zanna L., Amato E., Bucciantini N., 2004, A&A, 421, 1063
Del Zanna L., Zanotti O., Bucciantini N., Londrillo P., 2007, A&A, 473, 11
Duncan R. C., Thompson C., 1992, ApJ, 392, L9
Janka H.-T., Mueller E., 1995, ApJ, 448, L109
Kennel C. F., Coroniti F. V., 1984, ApJ, 283, 694
Kohri K., Narayan R., Piran T., 2005, ApJ, 629, 341
Komissarov S. S., Barkov M. V., 2007, MNRAS, 382, 1029
Komissarov S. S., Lyubarsky Y. E., 2004, MNRAS, 349, 779
Königl A., Granot J., 2002, ApJ, 574, 134
Lyubarsky Y. E., Eichler D., 2001, ApJ, 562, 494
MacFadyen A. I., Woosley S. E., 1999, ApJ, 524, 262
Maeda K., Nakamura T., Nomoto K., Mazzali P. A., Patat F., Hachisu I., 2002, ApJ, 565, 405
Matzner C. D., 2003, MNRAS, 345, 575
Mazzali P. A. et al., 2006, Nat, 442, 1018
McKinney C. J., Blandford R. D., 2009, MNRAS, 394, L126
Metzger B. D., Thompson T. A., Quataert E., 2007, ApJ, 659, 561
Nagataki S., Mizuta A., Yamada S., Takabe H., Sato K., 2003, ApJ, 596, 401
Nagataki S., Mizuta A., Sato K., 2006, ApJ, 647, 1255
Proga D., MacFadyen A. I., Armitage P. J., Begelman M. C., 2003, ApJ, 599, L5
Rhoads J. E., 1999, ApJ, 525, 737
Scheck L., Kifonidis K., Janka H.-T., Müller E., 2006, A&A, 457, 963
Sherwin B. D., Lynden-Bell D., 2007, MNRAS, 378, 409
Soderberg A. M., 2006, in Holt S. S., Gehrels N., Nousek J. A., eds, ASP Conf. Proc. 836, Gamma-Ray Bursts in the Swift Era. Astron. Soc. Pac., San Francisco, p. 386
Soderberg A. M., Nakar E., Berger E., Kulkarni S. R., 2006, ApJ, 638, 930
Thompson C., 1994, MNRAS, 270, 480
Thompson T. A., Burrows A., Meyer B. S., 2001, ApJ, 562, 887
Thompson T. A., Chang P., Quataert E., 2004, ApJ, 611, 380
Thompson T. A., Quataert E., Burrows A., 2005, ApJ, 620, 861
Tomimatsu A., Matsuoka T., Takahashi M., 2001, Phys. Rev. D, 64, 123003
Usov V. V., 1992, Nat, 357, 472
Uzdensky D. A., MacFadyen A. I., 2006, ApJ, 647, 1192
Uzdensky D. A., MacFadyen A. I., 2007, ApJ, 669, 546
Wheeler J. C., Yi I., Höflich P., Wang L., 2000, ApJ, 537, 810
Wheeler J. C., Maund J. R., Couch S. M., 2008, ApJ, 677, 1091
Woosley S. E., Bloom J. S., 2006, ARA&A, 44, 507
Woosley S. E., Weaver T. A., 1995, ApJS, 101, 181
Woosley S. E., Heger A., Weaver T. A., 2002, Rev. Mod. Phys., 74, 1015
Zhang B., 2007, Chin. J Astron. Astrophys., 7, 1

This paper has been typeset from a TeX/LaTeX file prepared by the author.